Robust Strategies for Automated AFM Force Curve Analysis—II: Adhesion-Influenced Indentation of Soft, Elastic Materials

David C. Lin
Laboratory of Integrative and Medical Biophysics,
National Institutes of Health,
9 Memorial Drive,
Building 9, Room 1E118,
Bethesda, MD 20892
e-mail: lindavid@mail.nih.gov

Emilios K. Dimitriadis
National Institute of Biomedical Imaging and Bioengineering,
National Institutes of Health,
13 South Drive,
Building 13, Room 3N17,
Bethesda, MD 20892
e-mail: dimitria@helix.nih.gov

Ferenc Horkay
Laboratory of Integrative and Medical Biophysics,
National Institutes of Health,
13 South Drive,
Building 13, Room 3W16,
Bethesda, MD 20892
e-mail: horkay@helix.nih.gov

*In the first of this two-part discourse on the extraction of elastic properties from atomic force microscopy (AFM) data, a scheme for automating the analysis of force-distance curves was introduced and experimentally validated for the Hertzian (i.e., linearly elastic and noninteractive probe-sample pairs) indentation of soft, inhomogeneous materials. In the presence of probe-sample adhesive interactions, which are common especially during retraction of the rigid tip from soft materials, the Hertzian models are no longer adequate. A number of theories (e.g., Johnson–Kendall–Roberts and Derjaguin–Muller–Toporov), covering the full range of sample compliance relative to adhesive force and tip radius, are available for analysis of such data. We incorporated Pietrement and Troyon's approximation (2000, "General Equations Describing Elastic Indentation Depth and Normal Contact Stiffness Versus Load," J. Colloid Interface Sci., **226**(1), pp. 166–171) of the Maugis–Dugdale model into the automated procedure. The scheme developed for the processing of Hertzian data was extended to allow for adhesive contact by applying the Pietrement–Troyon equation. Retraction force-displacement data from the indentation of polyvinyl alcohol gels were processed using the customized software. Many of the retraction curves exhibited strong adhesive interactions that were absent in extension. We compared the values of Young's modulus extracted from the retraction data to the values obtained from the extension data and from macroscopic uniaxial compression tests. Application of adhesive contact models and the automated scheme to the retraction curves yielded average values of Young's modulus close to those obtained with Hertzian models for the extension curves. The Pietrement–Troyon equation provided a good fit to the data as indicated by small values of the mean-square error. The Maugis–Dugdale theory is capable of accurately modeling adhesive contact between a rigid spherical indenter and a soft, elastic sample. Pietrement and Troyon's empirical equation greatly simplifies the theory and renders it compatible with the general automation strategies that we developed for Hertzian analysis. Our comprehensive algorithm for automated extraction of Young's moduli from AFM indentation data has been expanded to recognize the presence of either adhesive or Hertzian behavior and apply the appropriate contact model.*
[DOI: 10.1115/1.2800826]

Keywords: adhesive contact, atomic force microscopy, contact mechanics, elasticity, indentation

Introduction

In the first paper of this two-part series on automated analysis of atomic force microscopy (AFM) indentation data [1], we presented a comprehensive algorithm for extracting Young's moduli based on Hertzian contact mechanics. The Hertz theory and its subsequent expansions to include different geometries were used to model the contact between two elastic solids with no surface forces. The Hertzian models do not account for adhesive interactions between tip and sample and hence are inadequate in the presence of surface forces. In the context of AFM nanoindentation, the existence of surface forces causes the load-indentation behavior to deviate from the ideal Hertzian relationship.

Adhesive contact mechanics theories were pioneered by Johnson et al. [2] (Johnson–Kendall–Roberts or JKR theory), who modified the classical Hertz theory of contact between spherical bodies to account for the influence of surface energy. An alternative and apparently contradictory theory was formulated by Derjaguin et al. [3] (Derjaguin–Muller–Toporov or DMT theory). The seeming inconsistency was resolved by Tabor [4], who identified the applicability of the two theories to opposite extremes of the relationship between adhesive force and sample compliance; the JKR theory appertains to cases of strong adhesive forces and large tip radii relative to sample compliance, while the DMT theory is appropriate for weak adhesive forces and small tip radii relative to sample compliance (a more quantitative explanation can be found in Appendix A). Muller et al. [5] and Greenwood [6] used the Lennard–Jones potential in their numerical analyses of interactions in the intermediate regime. Maugis [7] was able to obtain closed-form solutions of the relationship between force, contact radius, and indentation in the intermediate regime by employing a Dugdale potential, which approximates the Lennard–Jones potential by a square well of constant attractive force. The Maugis–Dugdale (MD) model was made more tractable in application to actual indentation data by Carpick et al. [8], who developed a general equation relating force and contact radius (Carpick–Ogletree–Salmeron or COS equation) that closely approximates the MD model. Utilizing the same approach, Pietrement

Contributed by the Bioengineering Division for publication in the JOURNAL OF BIOMECHANICAL ENGINEERING. Manuscript received October 19, 2006; final manuscript received April 6, 2007. Review conducted by Clark T Hung.

and Troyon [9] generated a force-indentation relationship (Pietrement–Troyon or PT equation) that deviates from the MD model by 1% or less. The COS and PT equations therefore provide the means to effectively employ the MD model to experimental data.

In this work, we incorporate the PT equation for adhesive contact between a rigid spherical indenter and an elastic sample into the automated scheme introduced in the prior paper [1]. The various theories will first be presented, followed by a description of the strategies employed to integrate analysis of adhesive interactions into the existing scheme. We devote a portion of the paper to the detailed discussion of salient features of each model with respect to force-displacement data; such information is lacking in the literature but of great importance in applying the theories to experimental data. Values of Young's moduli are then compared for AFM indentation datasets processed with either the Hertzian model or the MD model. Polyvinyl alcohol (PVA) gel was selected as the model system for our studies on the basis of its reversibility, the ability to modulate its elastic modulus by systematically varying its composition, and its chemical neutrality.

Theory

Comparison of Contact Mechanics Models. The original Hertz theory and the aforementioned adhesive theories apply to spherical bodies under contact. The specific case of the indentation of a compliant surface by a rigid probe allows the relationships to be simplified. These simplified equations for the Hertz, JKR, DMT, and MD models, including the COS and PT approximations, are presented in Appendix A. The first column in Fig. 1 shows schematically the phases of importance in the Hertzian indentation process along with the general force-displacement curve at each phase. In the Hertz contact model given by Eqs. (A2) and (A3), both indentation depth d and applied force F_n are zero at the point of initial contact (during tip extension toward the sample surface) or the point of separation (also called the pull-off point for tip retraction from the sample surface). When adhesive (attractive) interactions are present, contact occurs under the influence of such forces. These nonzero interaction forces cause deflection of the cantilever toward the sample surface ($F_n<0$ in the adopted convention shown in Fig. 1, where concave bending is positive). Formally, the terms "attractive force" and "adhesive force" are used to differentiate between the external forces during tip extension and tip retraction, respectively [10]. We will dispense with the convention here and refer to both as adhesive forces.

The chief difference between the JKR and DMT theories given by Eqs. (A4)–(A7) and Eqs. (A8)–(A10), respectively, is the relation between the contact area and the applied force. In the DMT theory, the contact area becomes zero when the maximum adhesive force F_{ad} is balanced by the cantilever restoring force [11]. This occurs at the point of initial contact when the tip approaches the sample and at the pull-off point when the tip is retracted (see Fig. 1, second row from top). In the JKR theory, when $F_n=-F_{ad}$, the contact area is nonzero, resulting in abrupt contact or separation. In fact, the contact area is never zero in the JKR model, as clearly seen in Eq. (A5).

Another important distinction between the JKR and DMT theories can be discerned by comparing the indentation relationships given by Eqs. (A4) and (A8). In the JKR theory, the indentation at the point of contact or separation is negative, as shown by Eq. (A7) [12]. A negative indentation can be interpreted as deformation of the sample surface *toward* the probe (i.e., opposite in direction to the deformation due to Hertzian indentation), as seen in Fig. 1 (JKR, second row from top). The JKR theory is therefore suitable for modeling interactions between the tip and a much more compliant sample, in which the adhesive force is strong enough to overcome the sample stiffness and cause the surface to be drawn toward the tip. In the DMT model, the indentation δ vanishes at the point of contact or separation (i.e., $\delta=0$ at contact area $a=0$). Hence, the model represents the other extreme of sample compliance and applies to the indentation of relatively stiff samples. The DMT force-indentation relationship, derived by combining Eqs. (A8)–(A10), is essentially the Hertz relationship with the addition of the adhesive force term given by Eq. (A10). We note that the point of zero indentation in the JKR theory corresponds to an applied force of $F_n=-(8/9)F_{ad}$, where F_{ad} is the maximum adhesive force obtained by setting $\delta=0$ in Eq. (A4), substituting the definition of the contact area given by Eq. (A5), and solving for F_n. Hence, the point of zero indentation occurs after contact (during extension) or before separation (during retraction).

The MD theory, represented in its entirety by Eqs. (A11)–(A17), spans the intermediate regime between the JKR and DMT models; some amount of negative indentation is permitted, depending on the compliance of the sample. The model is tedious to apply in practice because the lack of a direct relationship between force and indentation requires numerical iterations for multiple fitting parameters. The empirical COS and PT equations fa-

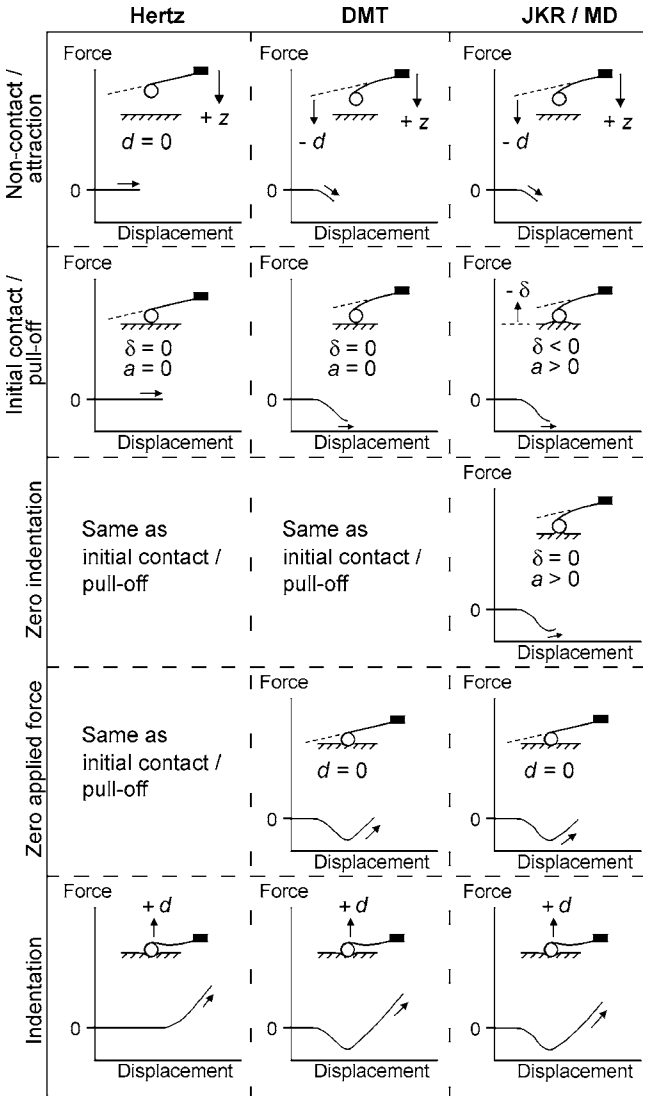

Fig. 1 Schematic of force-displacement behavior as predicted by the Hertzian, DMT, JKR, and MD theories. Force-displacement plots are shown for the approach portion of the cycle. The sign convention is as follows: piezo displacement *z* toward the sample surface is positive, convex bending of the cantilever (deflection *d* in direction of piezo motion) is negative, and convex deformation of the sample surface δ (initial contact or pull-off in the JKR and MD theories) is also negative.

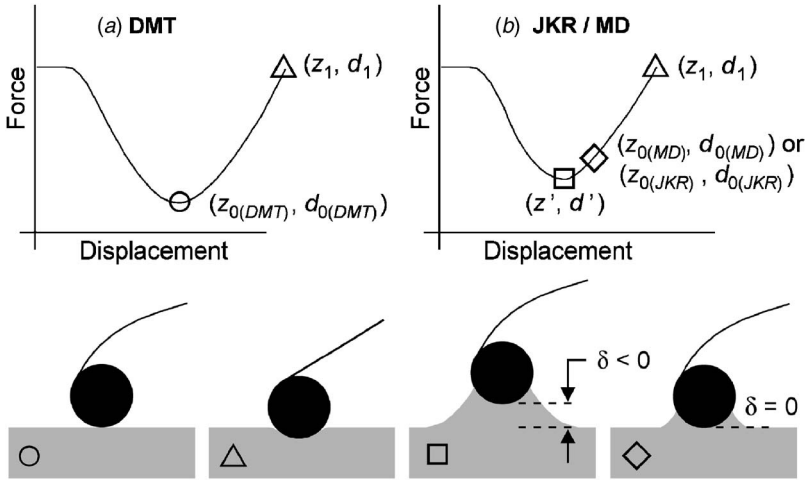

Fig. 2 Comparison of force-displacement behavior in the three adhesive contact models (DMT, JKR, and MD). Indentation is always zero at the point of contact in the DMT model (indicated by ○), but can be negative in the JKR and MD models (indicated by □) to allow for deflection of the sample surface toward the tip. Equally important in the JKR and MD models is the point of zero indentation (indicated by ◇), which is the reference point used to calculate indentation depth from the force-displacement data. In all three theories, the point of zero applied force (i.e., zero cantilever deflection, indicated by △) occurs at positive indentation depth.

cilitate direct fitting of indentation data to the MD model by establishing direct relationships between the applied force and either the contact radius or indentation. The COS equation represents the former relation and is given by Eq. (A18). For typical AFM indentation data, the PT equation given by Eq. (A20) may be used.

Essential Reference Points in Force-Displacement Curves. The AFM does not allow direct measurements of force and indentation depth. Despite the common use of the terms "force-displacement curve" and "force curve," AFM nanoindentation data are usually in the form of cantilever deflection (d) as a function of the position of the fixed end or base of the cantilever (z). Hence, reference points are necessary to convert the raw values to values of force and indentation. In the first paper of this two-part series [1], methods requiring the identification of the contact point were proposed as being more capable than contact point independent methods of handling diverse types of data. When adhesive interactions are present, reference points become crucial in the proper evaluation of adhesive and elastic behavior contained in the data. Because discussion of this detail is generally lacking in the literature, we describe here the essential reference points required to recast the force-indentation relationships into forms useful for analyzing AFM data; strategies for identifying these points will be presented in the next section. The applied force is directly related to the cantilever deflection through the spring constant of the cantilever (k_c) by

$$F_n = k_c(d - d_1) \tag{1}$$

where d_1 is the zero-deflection position of the cantilever. From our previous paper [1], the indentation is defined by

$$\delta = (z - z_0) - (d - d_0) = (z - d) - (z_0 - d_0) = w - w_0 \tag{2}$$

where the reference point (z_0, d_0) is the point of zero indentation. The transformed variable $w = z - d$ and its value at the reference point w_0 are introduced for simplification. Note the distinction between the point of zero external force (z_1, d_1) and the indentation reference point (z_0, d_0); the two points are coincident only in Hertzian mechanics. All reference points can be expressed in terms of z or w.

In the DMT model, both indentation depth and contact radius are zero at the point of contact (z_0, d_0) and increase with the externally applied load following Eq. (A8). In physical terms, the cantilever is permitted to deflect toward the sample surface prior to contact, reaching its maximum *negative* deflection or maximum attractive force at the point of contact (see Fig. 2). At the onset of contact in the JKR and (to a lesser extent) MD models, the tip and sample surface are instantaneously drawn together, resulting in a nonzero contact radius and negative indentation depth. The contact point in the JKR and MD models is denoted by (z', d') in Fig. 2. As in the DMT theory, contact occurs at the maximum attractive force F_{ad}.

It should be noted that quantitative methods based on adhesive interactions between the indenter tip and the sample have been developed by a number of researchers including Scheffer et al. [13], Eaton et al. [14], and Sun et al. [15]. For example, the approach of Sun et al., based on various adhesion theories, allows for the extraction of E based on contact radii at different depths of indentation. However, the PT equation is the most amenable to automation because its application to AFM indentation data requires only the identification of the three reference points shown in Fig. 2(*b*).

Cao et al. [16] used a depth-sensing nanoindentation system in their tests of polydimethylsiloxane and applied the JKR model and the PT equation to the fitting of the force-indentation data. Compared to the AFM, depth-sensing systems provide superior load control and displacement accuracy but lack the precise sample positioning and imaging capabilities afforded by the AFM [17]. In the study by Cao and colleagues, the contact point was assumed to be the point of zero indentation. Implicit in the assumption is that there is no deformation of the sample toward the tip (as in the DMT model) and that a contact area arises instantaneously upon contact between the tip and the sample surface. In our approach, we incorporate methods to treat the contact point and point of zero indentation separately in accordance with the MD theory; the provision for negative indentations is important for indentation behavior approaching the JKR limit.

Description of Algorithm for Automated Fitting of Indentation Data Using the Pietrement–Troyon Equation. We now discuss in depth the strategies employed to incorporate the key processes required to automatically fit indentation data using the PT

equation. An automated routine capable of accurately analyzing AFM indentation data regardless of whether adhesive interactions are present must be able to distinguish between datasets that exhibit Hertzian and adhesive behavior. Identifying adhesive contact from force-displacement curves is straightforward because of the pronounced negative deflection of the cantilever near the onset of initial contact. The following procedure is utilized to establish the existence of such interactions:

1. Marching along the dataset, the initial portion (noncontact region) is fitted with a line while the latter portion is fitted with a power function of the form
$$d = d^{(i)} + b(z - z^{(i)})^{3/2} \tag{3}$$
where b is the lone fitting parameter, i is the current iteration, and the exponent of 3/2 is characteristic of Hertzian indentation with a rigid sphere [18,19]. Hence, $(z^{(i)}, d^{(i)})$ takes on all values between the first $(i=1)$ and last points. In the adopted convention, the last point refers to the point of maximum indentation, regardless of whether extension or retraction data are considered.
2. At each iteration, an aggregate mean-square error (MSE) is calculated, with the contribution from the nonlinear fit given greater weight to offset the typically low MSE values from the zero-force, noncontact region. In most cases, multiplying the MSE of the nonlinear fit by a factor of 2 is sufficient. However, if the noncontact region comprises a disproportionately large segment of the data, a larger factor (e.g., 10) is necessary to identify the best fit to the contact region. The linear fit associated with the lowest aggregate MSE is used as a preliminary check for the presence of adhesive forces—a negative slope using either factor indicates that such interactions are potentially present. If the slopes using both factors are positive, Hertzian analysis is applied. The $(z^{(i)}, d^{(i)})$ pair corresponding to the lowest MSE is denoted (z^*, d^*). An example of the two-part fit of a typical retraction curve is shown in Fig. 3 (Dataset "a").
3. For a negative slope, the global minimum of the d versus z data is found. The position of this point is identified by its index $i=\kappa$. The minimum value of d is therefore designated by $d^{(\kappa)}$.
4. The data from $i=1,2,3,\ldots,\kappa$ is fitted with both a force law based on the Lennard–Jones potential (detailed in Appendix B) and a linear function. The MSE of each fit is computed.
5. If adhesive interactions are present, the force law provides a significantly better fit of the data than does the linear fit (see Example "b" in Fig. 3). In the absence of adhesive forces, $d^{(\kappa)}$ is attributed to intrinsic noise in the data, and the linear function will be the superior fit. In this case, the procedure again reverts to Hertzian analysis.
6. For adhesive contact, the external force reference d_1 from Eq. (1) is obtained from the Lennard–Jones fit as described in Appendix B. The postcontact force reference point (z_1, d_1) is found by a linear search in the interval bounded by $(z^{(\kappa)}, d^{(\kappa)})$ and the last point.

We use (z_1, d_1) to estimate the axial strain ε_{zz} using the Hertzian mechanics relation [20]
$$\varepsilon_{zz} = \frac{2\delta^{1/2}}{\pi R^{1/2}(1-\nu)} \tag{4}$$
While use of the Hertzian relationship and approximation of the Hertz contact point by (z_1, d_1) introduce errors in the computation, we use this approach to merely establish a rough threshold for linear stress-strain behavior. Some prior knowledge of the sample mechanical properties is beneficial since the linear regime is material dependent. Based on the specified strain limit, the portion of the data exceeding the threshold is excluded from the analysis.

In tip retraction, the minimum cannot simply be regarded as the pull-off point since multiple release points can arise due to events such as the unfolding of large molecules adsorbed to the tip and sample surfaces or the unbinding of multiple receptor-ligand pairs, leading to a "sawtooth" pattern in the d versus z curve [21]. In such cases, the MD theory is applicable from the initial release point (z', d'), as indicated in the typical example shown in Fig. 3 (Dataset "c"). This point may be difficult to locate accurately due to signal noise, but is generally in the vicinity of (z^*, d^*). Within the interval bounded by (z^*, d^*) and (z_1, d_1), the point corresponding to the smallest value of d, or the largest adhesive force, is taken to be the pull-off point (z', d'). Once the reference points (z', d') and (z_1, d_1) from Fig. 2(*b*) have been identified, the adhesive force can be calculated using Eq. (1) to be $F_{ad} = -k_c\,(d_1 - d')$ and compared to the maximum applied force F_{max} to determine whether the adhesive component can be neglected. Using the guideline set by Johnson and Greenwood [22], for $|F_{ad}/F_{max}| < 0.05$, Hertzian analysis is invoked.

Unlike (z', d') and (z_1, d_1), the location of the indentation reference point (z_0, d_0) is not readily established from conspicuous features of the force curve except in the limiting cases—it is congruent with the point of contact or separation in the DMT theory and corresponds to the point at which the applied force is equal to $-(8/9)F_{ad}$ in the JKR theory. In the intermediate regime governed

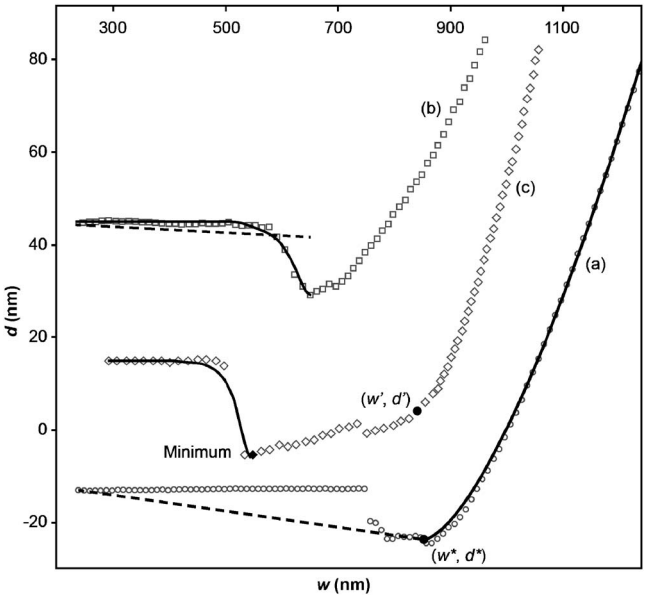

Fig. 3 (*a*) A typical retraction force curve fitted with a power function of 3/2 power (solid curve) and a line (dashed curve) joining the first point of the noncontact region and the first point of the power function. The negative slope of the line is indicative of significant adhesive interactions. For clarity, every fifth data point is shown. (*b*) Portion of a sample dataset (magnified 2×) showing a force law based on the LJ potential (solid curve) fitted to the noncontact segment of the data. The simple linear fit (dashed line) is also shown to demonstrate its comparatively poor fit when adhesive interactions are present. For clarity, every fourth point is shown. (*c*) Example of adhesive interactions during tip retraction that do not follow the LJ force law. The actual pull-off point (w', d') is clearly not the minimum, but rather the initial release point (not clear in the figure due to the small number of points plotted). The minimum in this case is the final release point. Note, however, that the force law still provides a superior fit of the data in the noncontact region than a linear function, and hence is still capable of identifying the presence of adhesive interactions. For clarity, every fourth data point is shown.

by the MD theory, we make use of the relationship between the applied force at zero indentation and the parameter α by setting Eq. (A20) to zero and manipulating to yield

$$\left.\frac{F_n}{F_{\text{ad}}}\right|_{\delta=0} = (F_n/F_{\text{ad}})_0 = [(1+\alpha)S^{3/(4-2\beta)} - \alpha]^2 - 1 \tag{5}$$

where S and β are defined by Eqs. (A24) and (A25), respectively. It can be verified that the ratio $(F_n/F_{\text{ad}})_0$ is exactly -1 for the DMT case ($\alpha=0$) and reaches a maximum value of -0.86 at $\alpha \approx 0.27$ before decreasing to $-8/9$ for the JKR case ($\alpha=1$).

Our strategy for finding (z_0, d_0) is to iteratively search for the value of α that yields the best fit of the data to Eq. (A20). In the interest of minimizing computation expense, it is important to consider the means by which the goodness of fit or MSE at each iteration is evaluated. The PT equation given by Eq. (A20), when expressed in the AFM-specific form by substituting Eq. (2) for δ and Eq. (1) for F_n, essentially casts z as a function of d. Hence, it is advantageous to reverse the roles of z and d as the independent and measured quantities, respectively, and use the measured values of d to calculate fitted values of z:

$$z = z_0 + d - d_0 + \frac{a_{0(\alpha)}^2}{R}\left\{\left[\frac{\alpha + \sqrt{1 + k_c(d-d_1)/F_{\text{ad}}}}{1+\alpha}\right]^{4/3} - S\left[\frac{\alpha + \sqrt{1 + k_c(d-d_1)/F_{\text{ad}}}}{1+\alpha}\right]^{2/3\beta}\right\} \tag{6}$$

The most direct approach to the data-fitting problem is to determine the values of $(F_n/F_{\text{ad}})_0$, d_0, z_0, and a_0 at each iteration of α by making use of known relations at the reference points. Note that the quantities $(F_n/F_{\text{ad}})_0$, α, and d_0 are related through Eqs. (1) and (5), while Eq. (A20) can be evaluated at $F_n=-F_{\text{ad}}$ and at $F_n=0$ to provide two additional equations for the two remaining unknowns z_0 and a_0. We reject this approach because it attempts to fit the data at only the three reference points rather than considering the complete dataset. There are two remaining approaches to generate the values of $(F_n/F_{\text{ad}})_0$, α, and d_0:

a. Each successive point $(w^{(i)}, d^{(i)})$ is assumed to be the indentation reference point. Equation (1) is then used to calculate $(F_n/F_{\text{ad}})_0$, which allows substitution of Eqs. (A24) and (A25) into Eq. (5) to generate the corresponding value of α and leaves a_0 as the lone fitting parameter in Eq. (6). Although this approach decreases complexity and computation time by eliminating z_0 as a fitting parameter, it is susceptible to large errors due to the low signal-to-noise ratios common in the vicinity of the contact/separation point (see sample Dataset "b" in Fig. 3).

b. The preferred method is to iteratively increment the value of α from 0 to 1 (we use a step size of 0.01). Equation (5) is applied at each iteration to calculate $(F_n/F_{\text{ad}})_0$ and Eq. (1) is then used to find d_0. Regression analysis is performed to determine values of the parameters z_0 and a_0 in Eq. (6).

Once the optimal location of (z_0, d_0) is found, Eq. (A22) is used to calculate the quantity $\bar{a}_0$ and the fitting parameter a_0^2/R yields the value of a_0. To determine the interfacial energy, Eq. (A23) is used to find $\bar{F}_{\text{ad}}$, which is then substituted with F_{ad} into Eq. (A16) to calculate γ. The elastic constant of the indented material K is then obtained from Eq. (A15). With K known, Young's modulus is calculated using Eq. (A1). The complete algorithm described in this section is represented by the flowchart in Fig. 4.

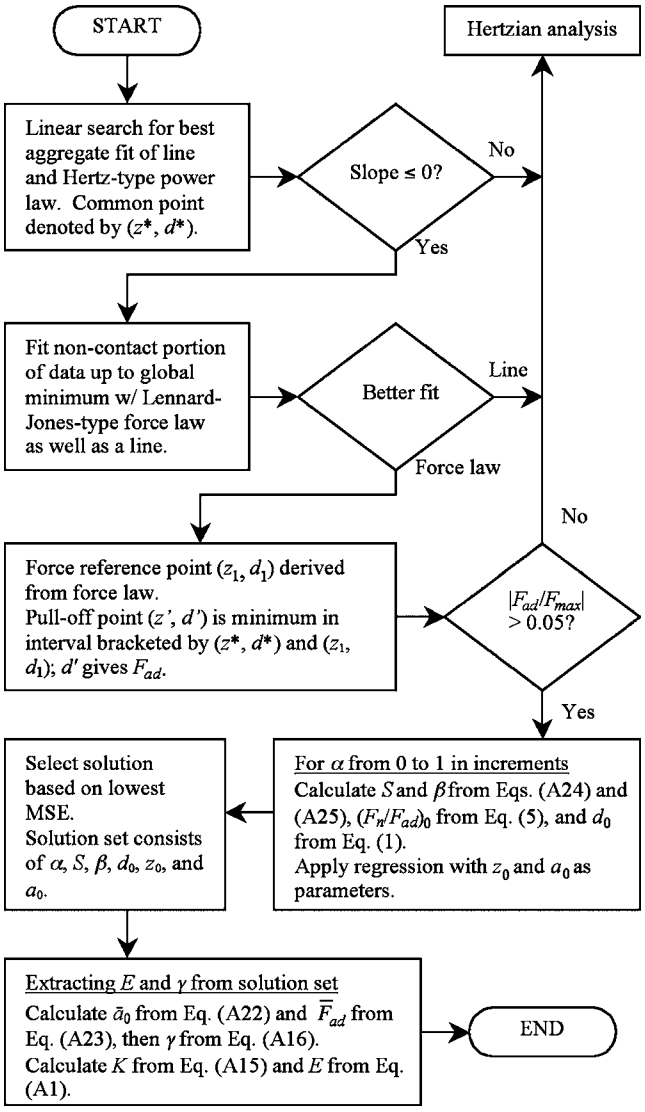

Fig. 4 Flowchart representing the comprehensive algorithm for processing AFM indentation data. Details on Hertzian analysis can be found in the previous paper [1].

Materials and Methods

The experimental details were described in our prior paper [1]. Testing of tissue-engineered cartilage will not be discussed here because no adhesive interactions were observed in the indentation of those samples. Briefly, PVA gel was cast into films (for AFM probing) or cylinders (for macroscopic compression testing) by varying the polymer content at constant cross-link density. The gels were cross-linked with glutaraldehyde at pH ~1.5, with an appropriate amount of cross-linker to ensure that all polymer chains were attached to a continuous network structure. All samples were fully swollen in water prior to testing.

A Texture Analyser bench top materials testing system (Stable Micro Systems, Surrey, UK) was used to perform dislacement-controlled compression of the gel cylinders (ramp speed of 1 mm/s or strain rate of 0.1/s until a preset load is achieved). Measurements were made at constant volume, with no detectable barreling. For all samples (at least three of each concentration), the shear modulus was determined from rubber elasticity theory [1,23,24].

Nanoindentation of samples was performed using a commercial AFM (Bioscope I with a Nanoscope IIIA controller, Veeco Instruments, Santa Barbara, CA) seated atop an inverted optical microscope. General purpose, oxide-sharpened silicon nitride tips were modified by gluing either a 9.6 μm diameter polystyrene bead or a 5.5 μm diameter glass bead near the tip. Multiple force curves for each PVA film were collected using the "force-volume" mode

Table 1 Comparison of Young's moduli from compression and AFM extension and retraction curves

Polymer content (%)	Macro. E[a] (kPa)	AFM (spherical tip)				
		E (Ext.)[a] (kPa)	E (Ret.)[a] (kPa)	Avg. α (Ret.)	E (Ret.)/ E (Ext.)[b]	Paired t test (0.05 level)
3	0.74±0.06	0.72±0.13	0.74±0.10	---	1.02±0.12	$t(511)=2.41$ $t_{critical}=1.96$
6	21.51±0.59	17.93±4.62	19.22±3.42	0.175	1.03±0.16	$t(511)=5.69$ $t_{critical}=1.96$
9	62.05±2.61	60.01±1.59	52.43±1.98	---	0.86±0.05	$t(1279)=158.28$ $t_{critical}=1.96$
12	115.50±1.86	113.66±6.06	108.98±9.17	0.050	0.96±0.10	$t(254)=7.59$ $t_{critical}=1.97$

[a]Expressed as the mean±standard deviation
[b]Outliers excluded from calculation for 6% gel.

of the AFM as described previously [1]. Each complete dataset consisted of 256 (16×16 raster scan) or 1024 (32×32 raster scan) sets of extension-retraction curves. Software developed in MATLAB (Mathworks, Natick, MA) and based on the algorithms described here and in the previous paper was used to automatically extract values of Young's modulus in extension and retraction. In all analyses, the data beyond an axial strain of roughly 20–25% were discarded.

Results and Discussion

Young's moduli from macroscopic compression and AFM extension data were presented previously [1] and are reproduced in Table 1 as well as in Fig. 5. For small adhesive force relative to indentation depth and applied force, the adhesive effects can be considered negligible and the indentation can be attributed solely to the externally applied load. This appeared to be the case in the extension curves, where attractive interactions were undetectably small and allowed all such data to be analyzed using Hertzian analysis. Data for retraction curves are also presented in Table 1 and Fig. 5. Regardless of whether the Hertzian or MD theory was applied in analyzing the retraction data, the agreement between the average extracted values of E in extension and retraction were generally good. The largest difference was found in the 9% gels,

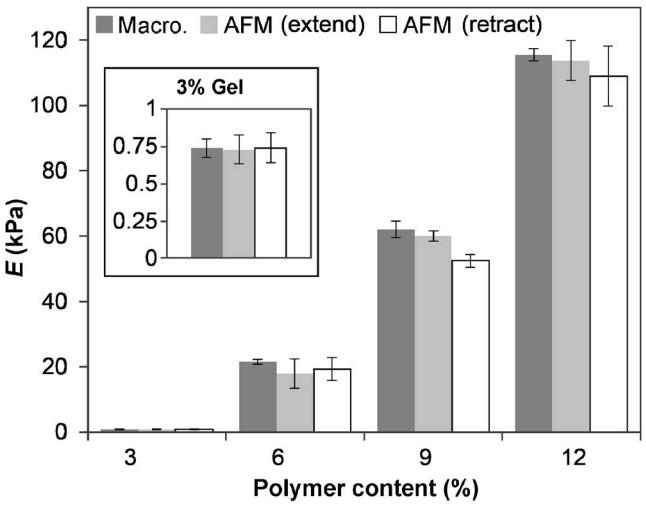

Fig. 5 Results of macroscopic compression and AFM indentation tests on PVA gels. Due to the large difference in sample size between AFM and macroscopic measurements, error bars show standard deviation rather than standard error. Extend and retract curves were analyzed for each AFM dataset and all datasets were restricted to ~25% strain.

where the average modulus in retraction was 12.6% smaller than the extension value. Average Young's moduli also compared favorably with the macroscopic results. The differences when comparing E in extension and retraction within an *individual* set of curves ranged from an average of 10.2% to 16.2%. This was expected as a consequence of the varying degrees of hysteresis present in each set of extension-retraction curves and is independent of the existence of adhesive effects. The statistical significance of the difference between extension and retraction data was evaluated using paired t tests, with the results reported in Table 1. Based on the results, there was significant difference between extension and retraction data in all the samples, indicating that hysteresis affects the mechanics of tip retraction regardless of the presence of adhesion. Although it may appear that analysis of retraction data serves mainly as a means of obtaining a quantitative measure of the level of hysteresis, it may be necessary in cases where the extension curve is intractable due to high levels of noise.

In the analysis of indentation data, strains were limited to approximately 20–25%. As reported in the previous paper, we found that when points representing axial strains close to 50% were included in the analysis, some strain hardening as indicated by increases in extracted Young's moduli and the residuals resulted. It is important to point out that the adhesive theories, which have their basis on the Hertz theory, are predicated on the assumption of linear stress-strain behavior. Regardless of the existence of significance adhesion, it is advisable to establish an estimate of the linear strain limit by performing preliminary indentations to different depths and establishing a base line of cantilever deflection. This can prevent unnecessary truncation of data to exclude nonlinear points that deviate from linear behavior.

Note that since the samples were made from the same batch, the variability in adhesive interactions from sample to sample was likely due to differences in the surface properties of the tips. The absence of significant adhesion in the 3% and 9% gels suggests that the polymer concentration does not affect the adhesion properties. With the choice of neutral PVA as the model system, we sought to eliminate excessive adhesion in order to ensure complete release of the tip following each indentation. The limited range in vertical travel z of the AFM used in the study, coupled with cantilevers of low bending stiffness, introduced the possibility of the tip being adhered to the sample even at maximum retraction. When probing samples that exhibit adhesive behavior, it is therefore important to verify the existence of noncontact regions in both extension and retraction force curves. The degree of accuracy in applying the PT equation to AFM indentation data then becomes largely a function of correctly identifying the reference points shown in Fig. 2. Even with disparate adhesive interactions and low signal-to-noise ratios near the pull-off point, our

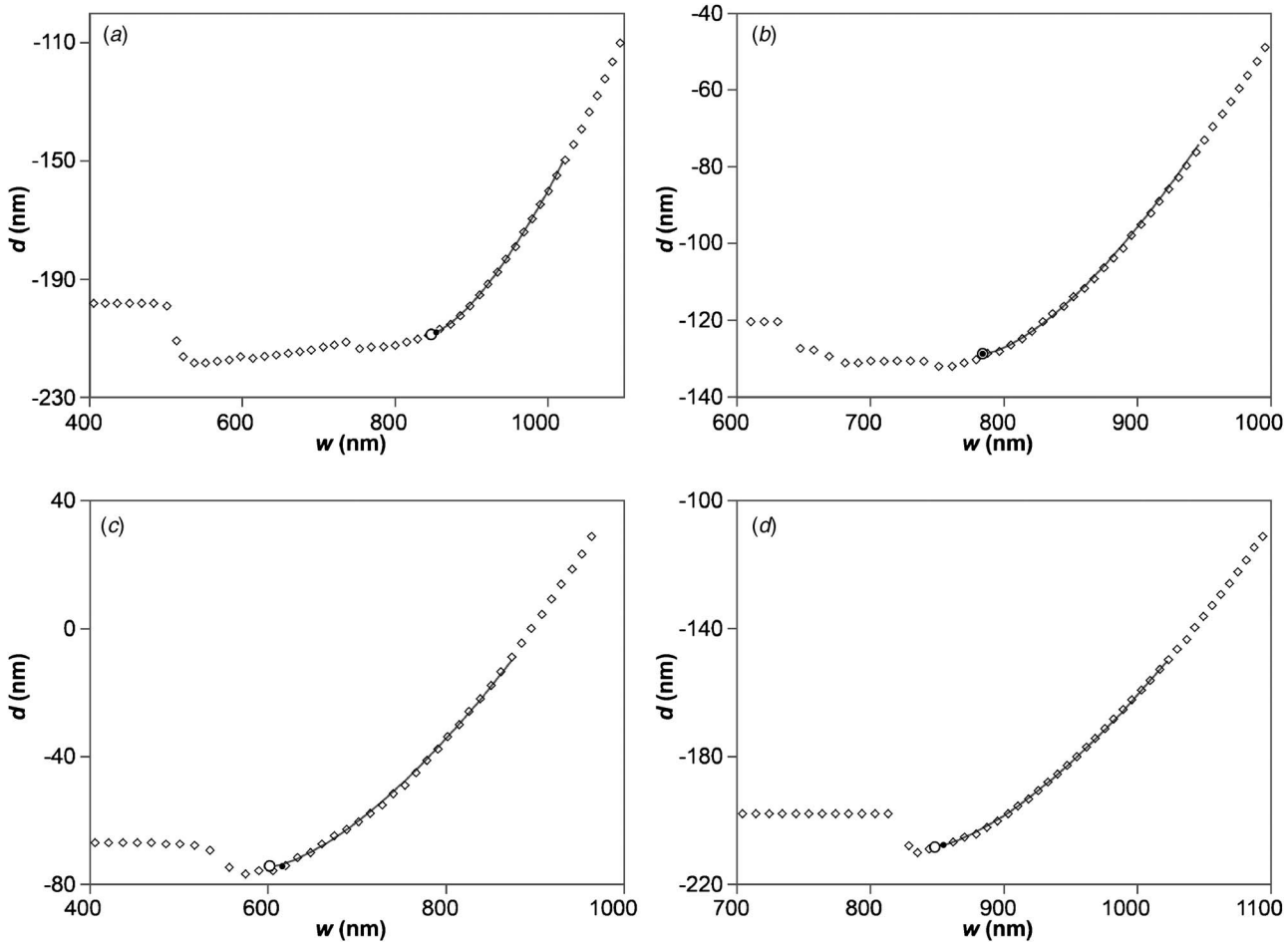

Fig. 6 Four representative retraction curves (every fifth to eighth point is plotted and indicated by ◇) showing disparate adhesive interactions. For the fitting, all datasets were restricted to ~25% strain. Fitted curves are represented by the solid lines. Also shown are the contact points (indicated by ○) and points of zero indentation (indicated by ●).

approach was capable of successfully finding the reference points. Some sample fits of retraction curves with the PT equation are shown in Fig. 6.

The dimensionless parameter α in the PT equation represents the extent to which the adhesive interactions approach those predicted by the JKR ($\alpha=1$) and DMT ($\alpha=0$) theories. It is also valuable as a secondary check of the accuracy of the PT equation in modeling the indentation mechanics. For stiff materials and low interfacial energies, α is expected to approach the DMT limit of 0 while soft materials with a propensity to deform toward the tip yield values of α that approach unity. These features are borne out in the indentation of the PVA gels, with $\alpha \sim 0.05$ for the stiffest gels (12% polymer content) and $\alpha \sim 0.18$ for the more compliant gels (6% polymer content).

Conclusions

We have successfully incorporated adhesive contact mechanics into the automated procedure we first introduced for Hertzian analysis of AFM data from the indentation of soft, chemically cross-linked gels. The PT approximation of the MD theory has been shown to be readily adaptable to the automation algorithm. The accuracy of the PT equation was demonstrated by the excellent agreement between the results from macroscopic compression and nanoindentation of PVA gels. The comprehensive scheme is capable of automatically detecting the presence of adhesive interactions and applying the appropriate contact mechanics model to the processing of AFM datasets. This capability should prove to be a valuable tool for the high-throughput processing of large collections of AFM datasets and may be particularly important in the probing of highly inhomogeneous materials.

Acknowledgment

This work was supported by the Intramural Research Program of the NIH/NICHD.

Appendix A: Equations Representing the Various Contact Models

The equations here are presented using the notation of Pietrement and Troyon [9], with subscripts (H), (JKR), (DMT), and (α) used to differentiate between the Hertz, JKR, DMT, and PT models, where ambiguity is not an issue, the subscripts can be dropped. The elastic constant K of the sample is defined by

$$K = 4E/3(1-\nu^2) \tag{A1}$$

where E and ν are Young's modulus and Poisson's ratio of the sample, respectively. The Hertz model gives the following relationships between force, indentation, and contact radius a [18]:

$$\delta = a_{(H)}^2/R \tag{A2}$$

$$a_{(H)} = (F_n R/K)^{1/3} \tag{A3}$$

where δ is the indentation, R is the radius of the probe, and F_n is the applied normal force.

The JKR model can be expressed by the following equations [2,9]:

$$\delta = \frac{a_{(\mathrm{JKR})}^2}{R} - \frac{4}{3}\sqrt{\frac{a_{(\mathrm{JKR})}F_{\mathrm{ad(JKR)}}}{RK}} \tag{A4}$$

$$a_{(\mathrm{JKR})} = \left[\frac{R}{K}\left(\sqrt{F_{\mathrm{ad(JKR)}}} + \sqrt{F_n + F_{\mathrm{ad(JKR)}}}\right)^2\right]^{1/3} \tag{A5}$$

$$F_{\mathrm{ad(JKR)}} = (3/2)\pi\gamma R \tag{A6}$$

where F_{ad} is the characteristic adhesive or pull-off force between the two surfaces and γ is the interfacial energy. Note that interfacial energy has units of energy per unit area (e.g., $\mathrm{J/m^2}$). At the point of contact or separation, when $F_n = -F_{\mathrm{ad}}$, the indentation is

$$\delta_{0(\mathrm{JKR})} = -\frac{1}{3}\frac{F_{\mathrm{ad(JKR)}}^{2/3}}{K^{2/3}R^{1/3}} \tag{A7}$$

The DMT theory gives [3,9]

$$\delta = a_{(\mathrm{DMT})}^2/R \tag{A8}$$

$$a_{(\mathrm{DMT})} = \left[\frac{R}{K}(F_n + F_{\mathrm{ad(DMT)}})\right]^{1/3} \tag{A9}$$

$$F_{\mathrm{ad(DMT)}} = 2\pi\gamma R \tag{A10}$$

The MD theory makes use of the nondimensional parameter λ given by [7,9]

$$\lambda = 2\sigma_0\left(\frac{R}{\pi K^2\gamma}\right)^{1/3} \tag{A11}$$

where σ_0 is the maximum attractive force in the Lennard–Jones potential and the Dugdale approximation. It is assumed that σ_0 exerts an influence over an area of radius c that is greater than the actual contact radius a. Regions of applicability of the DMT and JKR models are defined by $\lambda < 0.1$ (i.e., weak adhesive force and small tip radius relative to sample compliance) and $\lambda > 5$ (strong adhesive force and large tip radius relative to sample compliance), respectively. Note that λ is directly related to the parameter μ first introduced by Tabor [4] to define the ranges of applicability of the JKR and DMT theories by $\lambda = 1.16\mu$ [22]. In the intermediate regime $0.1 \leqslant \lambda \leqslant 5$, the MD equations are [7,9]

$$\frac{\lambda\bar{a}^2}{2}\left[(m^2-2)\tan^{-1}\sqrt{m^2-1} + \sqrt{m^2-1}\right] + \frac{4\lambda^2\bar{a}}{3}\left[\sqrt{m^2-1}\tan^{-1}\sqrt{m^2-1} - m + 1\right] = 1 \tag{A12}$$

$$\bar{F}_n = \bar{a}^3 - \lambda\bar{a}^2\left[\sqrt{m^2-1} + m^2\tan^{-1}\sqrt{m^2-1}\right] \tag{A13}$$

$$\bar{\delta} = \bar{a}^2 - \frac{4\lambda\bar{a}}{3}\sqrt{m^2-1} \tag{A14}$$

where $m = c/a$ and the contact radius, applied and adhesive force, and indentation have the nondimensionalized forms

$$\bar{a} = a\left(\frac{K}{\pi\gamma R^2}\right)^{1/3} \tag{A15}$$

$$\bar{F} = \frac{F}{\pi\gamma R} \tag{A16}$$

$$\bar{\delta} = \delta\left(\frac{K^2}{\pi^2\gamma^2 R}\right)^{1/3} \tag{A17}$$

The COS and PT equations are empirical approximations of the MD theory. The COS equation relates the contact radius to the external force and is given by [8,9]

$$\frac{a}{a_{0(\alpha)}} = \left(\frac{\alpha + \sqrt{1 + F_n/F_{\mathrm{ad}(\alpha)}}}{1+\alpha}\right)^{2/3} \tag{A18}$$

where $a_{0(\alpha)}$ is the contact radius at zero applied force and α is a nondimensional parameter related to λ by

$$\lambda = -0.924\ln(1 - 1.02\alpha) \tag{A19}$$

The limits of α are 0 for the DMT case and 1 for the JKR case. The PT equation relates indentation depth to the external force [9]:

$$\delta = \frac{a_{0(\alpha)}^2}{R}\left[\left(\frac{\alpha + \sqrt{1 + F_n/F_{\mathrm{ad}(\alpha)}}}{1+\alpha}\right)^{4/3} - S_{(\alpha)}\left(\frac{\alpha + \sqrt{1 + F_n/F_{\mathrm{ad}(\alpha)}}}{1+\alpha}\right)^{2\beta_{(\alpha)}/3}\right] \tag{A20}$$

The relationship between α and λ is now given by

$$\lambda = -0.913\ln(1 - 1.018\alpha) \tag{A21}$$

and the terms $a_{0(\alpha)}$, $F_{\mathrm{ad}(\alpha)}$, $\beta_{(\alpha)}$, and $S_{(\alpha)}$ are functions of α given by

$$\bar{a}_{0(\alpha)} = -0.451\alpha^4 + 1.417\alpha^3 - 1.365\alpha^2 + 0.950\alpha + 1.264 \tag{A22}$$

$$\bar{F}_{\mathrm{ad}(\alpha)} = 0.267\alpha^2 - 0.767\alpha + 2.000 \tag{A23}$$

$$S_{(\alpha)} = -2.160\alpha^{0.019} + 2.7531\alpha^{0.064} + 0.073\alpha^{1.919} \tag{A24}$$

$$\beta_{(\alpha)} = 0.516\alpha^4 - 0.683\alpha^3 + 0.235\alpha^2 + 0.429\alpha \tag{A25}$$

where the nondimensionalized forms of $a_{0(\alpha)}$ and $F_{\mathrm{ad}(\alpha)}$ are defined by Eqs. (A15) and (A16).

Appendix B: Fitting of Noncontact Data With the Lennard–Jones Potential

In AFM indentation data representing the attraction between a spherical probe and a flat surface, the portion of the data prior to initial contact or immediately following separation is oftentimes assumed to be governed by a force law similar to the Lennard–Jones (LJ) potential [22]. Formally, the LJ function governing the interaction between two rigid spheres is of the form

$$V(r) = 4\chi\left[\left(\frac{D}{r}\right)^{12} - \left(\frac{D}{r}\right)^{6}\right] \tag{B1}$$

where V is the potential, r is the separation distance, χ is the well depth, and D is the diameter of the spheres. Note that attractive forces are represented by negative potentials and that repulsive forces become dominant as the separation distance approaches zero. The latter feature of the LJ potential is ignored in the fitting of indentation data. Abandoning the formal representations, d is substituted for the potential V, and 4χ and D are replaced by generalized constants A and B, respectively.

It is necessary to transform the AFM data (d versus w) to the numerical form required by Eq. (B1). First, because increasing w corresponds to decreasing separation, the separation can be expressed nondimensionally by

$$r = 1 + C\frac{w^{(\kappa)} - w}{w^{(\kappa)}} \tag{B2}$$

where C is a scale factor that controls the rate at which the potential drops to its minimum value and κ refers to the point at which d is a minimum. Note that the separation at maximum attractive force has been set to unity for simplicity. A second transformation is performed to force d to conform to the behavior dictated by the LJ potential (i.e., at large separation, the potential is essentially zero). This is easily achieved by shifting the vector

of d values by a reference value (d_{ref}) equal to the maximum value of d in the range $d^{(1)}$ to $d^{(\kappa)}$. The force law is given by

$$d(r) = A\left[\left(\frac{B}{r}\right)^{12} - \left(\frac{B}{r}\right)^{6}\right] + d_{\text{ref}} \tag{B3}$$

To find the constants A and B, the equation $\partial d/\partial r = 0$ is solved at the minimum separation distance $r=1$ to give $B=(1/2)^{1/6}$. Equation (B3) is then be solved for A at the minimum $d^{(\kappa)}$, to yield $A=-4(d^{(\kappa)}-d_{\text{ref}})$.

We iteratively fit Eq. (B3) to subsets of data points from $(w^{(i)},d^{(i)})$ to $(w^{(\kappa)},d^{(\kappa)})$, where i is increased from 1 to κ and the scale factor C is the sole fitting parameter. Points prior to $(w^{(i)},d^{(i)})$ are fit to the line $d=d^{(i)}$. The value of $d^{(i)}$ corresponding to the best least-squares fit of the data is the zero-force reference d_1 in Eq. (1). Figures 4 and 5 show the results of fitting the force law to sample datasets.

References

[1] Lin, D. C., Dimitriadis, E. K., and Horkay, F., 2007, "Robust Strategies for Automated AFM Force Curve Analysis: I. Non-Adhesive Indentation of Soft, Inhomogeneous Materials," ASME J. Biomech. Eng. **129**(3), pp. 430–440.

[2] Johnson, K. L., Kendall, K., and Roberts, A. D., 1971, "Surface Energy and the Contact of Elastic Solids," Proc. R. Soc. London, Ser. A, **324**(1558), pp. 301–313.

[3] Derjaguin, B. V., Muller, V. M., and Toporov, Y. P., 1975, "Effect of Contact Deformations on the Adhesion of Particles," J. Colloid Interface Sci., **53**(2), pp. 314–326.

[4] Tabor, D., 1976, "Surface Forces and Surface Interactions," J. Colloid Interface Sci., **58**(1), pp. 2–13.

[5] Muller, V. M., Yushchenko, V. S., and Derjaguin, B. V., 1980, "On the Influence of Molecular Forces on the Deformation of an Elastic Sphere and Its Sticking to a Rigid Plane," J. Colloid Interface Sci., **77**(1), pp. 91–101.

[6] Greenwood, J. A., 1997, "Adhesion of Elastic Spheres," Proc. R. Soc. London, Ser. A, **453**(1961), pp. 1277–1297.

[7] Maugis, D., 1992, "Adhesion of Spheres: The JKR-DMT Transition Using a Dugdale Model," J. Colloid Interface Sci., **150**(1), pp. 243–269.

[8] Carpick, R. W., Ogletree, D. F., and Salmeron, M., 1999, "A General Equation for Fitting Contact Area and Friction Vs Load Measurements," J. Colloid Interface Sci., **211**(2), pp. 395–400.

[9] Pietrement, O., and Troyon, M., 2000, "General Equations Describing Elastic Indentation Depth and Normal Contact Stiffness Versus Load," J. Colloid Interface Sci., **226**(1), pp. 166–171.

[10] Burnham, N. A., Colton, R. J., and Pollock, H. M., 1991, "Interpretation Issues in Force Microscopy," J. Vac. Sci. Technol. A, **9**(4), pp. 2548–2556.

[11] Horn, R. G., Israelachvili, J. N., and Pribac, F., 1987, "Measurement of the Deformation and Adhesion of Solids in Contact," J. Colloid Interface Sci., **115**(2), pp. 480–492.

[12] Sarid, D., Hunt, J. P., Workman, R. K., Yao, X., and Peterson, C. A., 1998, "The Role of Adhesion in Tapping-Mode Atomic Force Microscopy," Appl. Phys. A: Mater. Sci. Process., **66**(1), pp. S283–286.

[13] Scheffer, L., Bitler, A., Ben-Jacob, E., and Korenstein, R., 2001, "Atomic Force Pulling: Probing the Local Elasticity of the Cell Membrane," Eur. Biophys. J., **30**(2), pp. 83–90.

[14] Eaton, P., Smith, J. R., Graham, P., Smart, J. D., Nevell, T. G., and Tsibouklis, J., 2002, "Adhesion Force Mapping of Polymer Surfaces: Factors Influencing Force of Adhesion," Langmuir, **18**(8), pp. 3387–3389.

[15] Sun, Y., Akhremitchev, B., and Walker, G. C., 2004, "Using the Adhesive Interaction between Atomic Force Microscopy Tips and Polymer Surfaces to Measure the Elastic Modulus of Compliant Samples," Langmuir, **20**(14), pp. 5837–5845.

[16] Cao, Y., Yang, D., and Soboyejoy, W., 2005, "Nanoindentation Method for Determining the Initial Contact and Adhesion Characteristics of Soft Polydimethylsiloxane," J. Mater. Res., **20**(8), pp. 2004–2011.

[17] Asif, S. A. S., Colton, R. J., and Wahl, K. J., 2001, "Nanoscale Surface Mechanical Property Measurements: Force Modulation Techniques Applied to Nanoindentation," *Interfacial Properties on the Submicrometer Scale*, J. Frommer and R. M. Overney, eds., ACS/Oxford University Press, Washington, pp. 198–215.

[18] Barber, J. R., 2002, *Elasticity*, Kluwer Academic, Dordrecht.

[19] Beatty, M. F., and Usmani, S. A., 1975, "On the Indentation of a Highly Elastic Half-Space," Q. J. Mech. Appl. Math., **28**(1), pp. 47–62.

[20] Dimitriadis, E. K., Horkay, F., Maresca, J., Kachar, B., and Chadwick, R. S., 2002, "Determination of Elastic Moduli of Thin Layers of Soft Material Using the Atomic Force Microscope," Biophys. J., **82**(5), pp. 2798–2810.

[21] Heinz, W. F., and Hoh, J. H., 1999, "Spatially Resolved Force Spectroscopy of Biological Surfaces Using the Atomic Force Microscope," Trends Biotechnol., **17**(4), pp. 143–150.

[22] Johnson, K. L., and Greenwood, J. A., 1997, "An Adhesion Map for the Contact of Elastic Spheres," J. Colloid Interface Sci., **192**(2), pp. 326–33.

[23] Horkay, F., and Nagy, M., 1980, "Elasticity of Swollen Polyvinyl Alcohol and Poly(Vinyl Acetate) Networks," Polym. Bull. (Berlin), **3**(8–9), pp. 457–463.

[24] Treloar, L. R. G., 1975, *The Physics of Rubber Elasticity*, Oxford University Press, Oxford.